

# Imprints of mass accretion on properties of galaxy clusters

Andreas Faltenbacher<sup>1,5</sup>, Brandon Allgood<sup>2</sup>, Stefan Gottlöber<sup>3</sup>, Gustavo Yepes<sup>4</sup> and Yehuda Hoffman<sup>5</sup>

<sup>1</sup>*UCO/Lick Observatory, University of California at Santa Cruz, 1156 High Street, Santa Cruz, CA 95064, USA*

<sup>2</sup>*Physics Dept., University of California at Santa Cruz, 1156 High Street, Santa Cruz, CA 95064, USA*

<sup>3</sup>*Astrophysikalisches Institut Potsdam, An der Sternwarte 16, 14482 Potsdam, Germany*

<sup>4</sup>*Grupo de Astrofísica, Universidad Autónoma de Madrid, Madrid E-280049, Spain*

<sup>5</sup>*Racah Institute of Physics, Hebrew University, Jerusalem 91904, Israel*

2 December 2024

## ABSTRACT

We use a large scale N-body simulation of the flat  $\Lambda$ CDM universe, including adiabatic gas dynamics (GADGET), to investigate the impact of mass accretion modes of galaxy clusters on the vector quantities, orientation and angular momentum. Our cluster sample comprises the 3000 most massive friends-of-friends halos found in the  $500 h^{-1}$ Mpc simulation box. We use the mass ratios of the two most massive progenitors at  $z = 0.5$   $m_2/m_1$  ( $m_1 \geq m_2$ ) to construct two accretion mode sub-samples, a recent major merger sample and a steady accretion mode sample. We find that the mass of current clusters in the merger sample is on average  $\sim 43\%$  larger than the mass of the two progenitors ( $m_1 + m_2$ ), whereas in the steady accretion mode sample a smaller increase of  $\sim 25\%$  is found. We show that the separation vector connecting the two most massive progenitor halos at  $z = 0.5$  is strongly correlated with the orientation of the current cluster. We also find that the current angular momentum in the recent major merger sample tends to be parallel to orbital angular momentum of the progenitors, whereas the angular momentum of the steady accretion mode sample is mainly determined by the angular momentum of the most massive progenitor. Finally we confirm the long range of correlations for the major and the minor principal axes ( $\lesssim 100 h^{-1}$ Mpc) and angular momentum ( $\lesssim 20 h^{-1}$ Mpc) for the dark matter as well as the gaseous component of galaxy clusters. A separate analysis of the two sub-samples indicates that the long range correlations are independent of the mass accretion mode.

**Key words:** large-scale structure of the Universe – methods: numerical,statistical – galaxies:clusters,general

## 1 INTRODUCTION

Alignment of galaxy cluster orientations has been controversial since Binggeli (1982). Using a sample of 44 Abell clusters he showed that clusters of galaxies are highly eccentric and oriented relative to neighbouring clusters at least for separations smaller than  $15 h^{-1}$ Mpc. Further he found anisotropies in the cluster distribution on scales up to  $50 h^{-1}$ Mpc. The first investigations using X-ray contours of the ionised gas trapped in the gravitational potential well of clusters led to no (Ulmer et al. 1989) or only weak (Rhee & Latour 1991) significance of alignment effects. However, Chambers et al. (2002) exploring X-ray position angles of 45 clusters found significant alignment of clusters’ orientations with the connecting line to the next neighbour for separations of  $\leq 20 h^{-1}$ Mpc. Analysing a large set of optical data on 637 Abell clusters Plionis (1994) found highly significant align-

ment effects on scales below  $10 h^{-1}$ Mpc that become weaker but extend up to  $150 h^{-1}$ Mpc.

In the literature two slightly different scenarios are proposed to explain the alignment of the orientation of clusters. Binney & Silk (1979) suggested that tidal interactions of evolving proto-cluster systems may lead to the growth of anisotropies of clusters and to relative orientation effects. However, West (1994) found that clusters grow by accretion and merging of surrounding matter that falls into the deep cluster potential wells along sheet-like and filamentary high density regions. van Haarlem et al. (1997) used numerical simulations of CDM models to demonstrate that clusters are elongated along the incoming direction of the last major merger. Further West & Blakeslee (2000) show that Virgo’s brightest elliptical galaxies have a remarkably collinear arrangement in three dimensions which is aligned with the filamentary structure connecting Virgo and the rich cluster

arXiv:astro-ph/0501452v1 20 Jan 2005

Abell 1367. In a statistical investigation of 303 Abell clusters Plionis et al. (2003) confirm the alignments of galaxy members with their parent cluster orientation as well as with the large-scale environment within which the clusters are embedded. Therefore, the cluster formation is tightly connected with the supercluster network that characterises the large-scale matter distribution in the universe. High-resolution simulations showing this effect were described by the Virgo collaboration, Colberg et al. (2000). Onuora & Thomas (2000) found a significant alignment signal up to scales of  $30 h^{-1}\text{Mpc}$  for a  $\Lambda\text{CDM}$  model. Faltenbacher et al. (2002) and Hopkins et al. (2005) using large scale dissipationless N-body simulations of the  $\Lambda\text{CDM}$  universe report alignment of the orientations of galaxy clusters for separations  $\lesssim 100 h^{-1}\text{Mpc}$ .

The angular momentum is a further vector quantity of galaxy clusters easily accessible in numerical simulations. Its orientation can be used to gain insight into the processes of mass accretion and tidal interactions with the large scale structure. According to Doroshkevich (1973), Peebles (1980), and White (1984) the primary angular momentum of bound objects is due to tidal interaction between the elongated proto-structures after decoupling from cosmic expansion and before turn-around. More recent studies find that the angular momentum of dark matter halos is later modified by the merging history of their building blocks, see Vitvitska et al. (2002) and Porciani et al. (2002a,b).

To link the vector quantities of galaxy clusters with the mass accretion modes we first locate the two most massive progenitor halos at  $z = 0.5$  for our simulated cluster sample. This sample comprises the 3000 most massive CDM halos found by a friends-of-friends (FoF) approach. We create two sub-samples, namely a recent major merger sample and a steady accretion mode sample. Within these sub-samples the imprint of the infall pattern of the two most massive progenitors on the current vector quantities (namely the principal axes and angular momentum) of clusters is studied. A strong correlation between the infall pattern and these vector quantities is obtained, indicating that the infall along the filaments determines the vector valued properties of the clusters. The interplay between the filamentary network on the one side and the clusters on the other side is then explored by the analysis of long range correlations of these vector quantities between cluster pairs.

The paper is organised as follows. §2 describes the simulation and explains the construction of cluster sample. In §3 the impact of different mass accretion modes (merger/steady accretion) on shape and angular momentum of the clusters is investigated. In §4 the range of the alignment of the major, the minor, and the angular momentum axes of cluster pairs is measured. §5 summaries the results.

## 2 SIMULATION AND CLUSTER SAMPLE

In subsection §2.1 we describe the simulation parameters. Then in §2.2 the construction of the basic cluster sample is described. And in the last subsection (§2.3) the subdivision into a merger and a steady accretion mode sample is explained.

### 2.1 Simulation

The simulation is performed using the GADGET code provided by Springel et al. (2001). According to the presently favoured cosmological model, we assume a flat universe with the parameters  $\Omega_m = 0.3$ ,  $\Omega_\Lambda = 0.7$  and a Hubble constant of  $h_{100} = 0.7$ . The linear power spectrum of the density fluctuations has been normalised to  $\sigma_8 = 0.9$ . The simulation is realized within a cube of  $500 h^{-1}\text{Mpc}$  edge size. The cold dark matter (CDM) and the gaseous component are represented by  $256^3$  particles each. The mean baryonic mass fraction of the universe is assumed to be  $\Omega_b/\Omega_m = 0.13$ , consequently the mass of a single CDM particle is  $m_{\text{dark}} = 5.4 \times 10^{11} h^{-1}M_\odot$  and the mass of a single gas particle is  $m_{\text{gas}} = 8.1 \times 10^{10} h^{-1}M_\odot$ . In the simulation the gas is treated adiabatically, hence no dissipative processes are taken into account.

### 2.2 Basic cluster sample

For the identification of cluster halos we apply a standard friends-of-friends (FoF) algorithm. The CDM and the gaseous particle distributions are treated separately. The basic cluster sample comprises the 3000 largest CDM particle halos found with a linking length of  $b = 0.17 \times l$ , where  $l$  is the mean particle distance (see eg. Jenkins et al. 2001). Subsequently the gaseous halos, identified by an analogous FoF approach applied to the gas particle distribution, are associated to the CDM clusters.

### 2.3 Mass accretion modes

For each of the 3000 clusters at  $z = 0$  we locate the two most massive progenitors at  $z = 0.5$ . This redshift for the progenitors is chosen based on the work of Suwa et al. (2003) (see also Richstone et al. 1992) which shows the formation rate of galaxy clusters in  $\Lambda\text{CDM}$  peaks at  $z \approx 0.4$ . In the following we compare the properties of clusters according to their accretion history. Therefore, we apply a simple scheme to distribute the clusters into sub-samples according to accretion mode. The criterion to divide the whole cluster sample into sub-samples is based on the mass fraction of the two most massive CDM progenitors  $m_2/m_1$ , where  $m_1$  and  $m_2$  denote the most and the second most massive progenitor, respectively. The upper panel of Fig. (1) shows the distribution of mass fractions  $((m_1 + m_2)/m_0)$  versus  $m_2/m_1$  with the steady accretion mode clusters appearing on the left and the recent major merger clusters appearing on the right.  $m_0$  denotes the mass of the emerged cluster at  $z = 0$ . The intermediate accretion mode clusters, which are not investigated in the following, are located in the middle of this panel (grey area). The boundaries in  $m_2/m_1$  separating the sub-samples are chosen in such a way, that each sub-sample comprises 1000 member clusters. The criterion using only the mass fractions of the progenitors at  $z = 0$  might be a harsh simplification, but all more complicated separation schemes (using for instance information about the final mass  $m_0$ ) unavoidably introduce some additional arbitrariness. The mean values of the fractions  $(m_1 + m_2)/m_0$  indicated by the horizontal lines in the upper panel of Fig. 1 are  $\sim 24\%$  lower in the merger sample compared to the steady accretion sample, whereas  $m_0$  is  $\sim 18\%$  higher in the merger sample

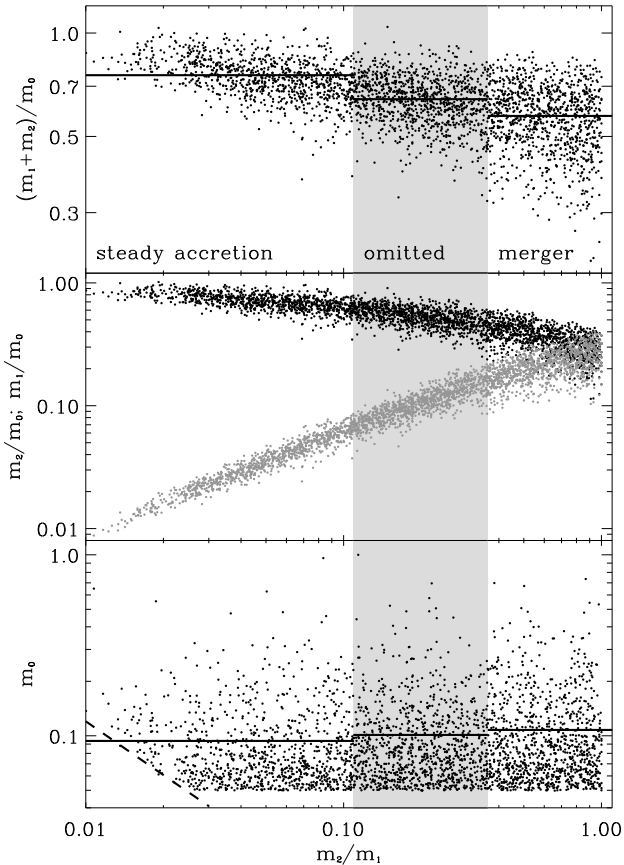


**Figure 1.** The masses of the clusters at  $z = 0$  are denoted by  $m_0$  and the masses of the two most massive progenitors at  $z = 0.5$  are denoted with  $m_1$  and  $m_2$ , respectively ( $m_1 \geq m_2$ ). The upper panel shows the ratio of the combined mass  $m_1 + m_2$  divided by  $m_0$  in dependence of  $m_2/m_1$ . In the middle panel the ratios of  $m_1/m_0$  and  $m_2/m_0$  (black and gray dots, respectively) are shown. The lower panel represents the normalised masses of the clusters at  $z = 0$ . The shaded area entitled 'omitted' contains the 1000 clusters with the intermediate ratios of  $m_2/m_1$ , whereas 'merger' and 'steady' indicate the sub-samples with the highest and lowest  $m_2/m_1$  respectively. The horizontal lines in the upper and lower panels indicate the mean values of the according sub-samples, 0.75, 0.64, 0.57 for the upper and 0.09, 0.10, 0.11 in for lower panel. The dashed line in the lower panel marks the boundary of completeness, below this line the second most massive progenitors comprise less than 5 particles.

compared to the steady accretion sample. The difference in the relative decrease of  $(m_1 + m_2)/m_0$  and the increase of  $m_0$  indicates a slightly higher additional accretion activity in the merger sample. The increase of  $m_0$  indicates that equal mass mergers tend to result in more massive halos. But they also show slightly enhanced accretion activity as indicated by the larger relative decrease of the mean values of  $(m_1 + m_2)/m_0$  compared to the relative increase of  $m_0$ . Of course these two characteristics (more massive descendants, slightly higher additional accretion) are closely related.

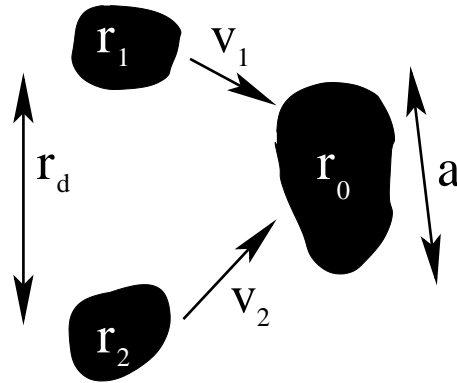


**Figure 2.** The sketch depicts the vectors used to describe the geometry of the accretion process.  $\mathbf{r}_1$  and  $\mathbf{r}_2$  are the locations of the two most massive progenitors at  $z = 0.5$ , the vector  $\mathbf{r}_d$  is the displacement vector between these two and  $\mathbf{a}$  marks the orientation of the principal axis of the cluster at  $z = 0$  (double arrows indicate that only the direction not the sign is considered here). The vectors  $\mathbf{v}_1$  and  $\mathbf{v}_2$  are the velocities of the progenitors as given in equation (3.1).

### 3 IMPACT OF ACCRETION MODES ON VECTOR QUANTITIES OF CLUSTERS

In this section we investigate the impact of the infall pattern on the vector quantities, i.e. principal axes and the angular momentum of the mass distribution. First we define some useful vectors which are related to the locations and velocities of the two most massive progenitor halos at  $z = 0.5$ . In the subsequent parts the correlation of these vectors with the shape and the angular momentum of current clusters is examined.

#### 3.1 Infall pattern

For the illustration of the infall pattern we use only the clusters in the recent major merger sample (see § 2.3). The vector quantities, which are later correlated with the shape and the angular momentum of the emerged cluster, are combinations of the position vectors of the two most massive progenitors  $\mathbf{r}_1$  and  $\mathbf{r}_2$  at  $z = 0.5$  and of the emerged cluster  $\mathbf{r}_0$  at  $z = 0$ . Of particular interest are the difference vector  $\mathbf{d}_r$  and the cross product of the velocities  $\mathbf{v}_\times$  as defined in the following equations.

$$\mathbf{r}_d = \mathbf{r}_1 - \mathbf{r}_2 \quad (1)$$

$$\mathbf{v}_\times = \mathbf{v}_1 \times \mathbf{v}_2, \quad (2)$$

where

$$\mathbf{v}_i = \frac{\mathbf{r}_0 - \mathbf{r}_i}{\Delta t} \quad i = 1, 2$$

$\mathbf{r}_d$  is the difference vector of the locations of the two most massive progenitor halos at  $z = 0.5$ . The directions of the mean velocities  $\mathbf{v}_1$  and  $\mathbf{v}_2$  are calculated by subtracting the position of the emerged cluster at  $z = 0$  by the according positions of the progenitors at  $z = 0.5$ . Thus  $\mathbf{v}_\times$  indicates the vector perpendicular to the orbital plane of the merging progenitors. In Fig. 2 the relevant vector quantities are sketched. The definition of  $\mathbf{v}_\times$  might be somewhat problematic since it does not refer to the actual velocities close to the

merging point. However since we use only the direction of the cross product for the following analysis, this inaccuracy does not influence the result.

Here we examine the tracks within the recent major merger sample to assure that the description of the infall pattern by  $\mathbf{r}_d$  and  $\mathbf{v}_\times$  is justified. We restrict our analysis to the recent major merger sample, since tracking the steady accretion mode involves following progenitors contain only a sparse number of particles, which are influenced by numerical effects. Before we display the overall pattern of infall in Fig. 4 we show in Fig. 3 two examples of the projection and the adjustment procedures which are applied before all the tracks can be compared to each other. Starting at  $z = 0.5$  we trace the tracks of the two progenitors, by computing the FoF halos for 33 simulation outputs between  $z = 0.5$  and  $z = 0$  and identify the descendant of each halo in the subsequent snapshot. For this exercise the following formula proved useful (for details see appendix A).

$$\alpha = \left[ 1 - \frac{|m_a - m_b|}{m_a + m_b} \right] \times \frac{m_o}{m_a}$$

Here  $m_a$  and  $m_b$  are the masses of the progenitor halo and descendant candidates respectively.  $m_o$  denotes the mass of particles which are found in both of the halos. The halo which results in the maximum value of  $\alpha$  is chosen to be the descendant. The tracks found by this procedure are projected onto the *merging plane* confined by the locations of the two most massive progenitors  $\mathbf{r}_1, \mathbf{r}_2$  and the position of the emerged cluster at  $\mathbf{r}_0$ . In Fig. 3 (right panels) the projection of the tracks of two different merging events onto the merging plane are shown. Each dot represents the location of the particular halo at a given snapshot. The planes are rotated in such a way that the positions of the two progenitors are located on the y-axis with equal separation from the origin. The y-coordinate of the most massive progenitor has positive y-values, the second massive progenitor is placed on negative y-values. In a second step (right panels of Fig. 3) the image is stretched in such a manner, that the initial coordinates of the progenitors remain unchanged but the final cluster position is projected to the x-axis. Additionally the merger point is shifted to the origin. This shifting neither changes the direction of  $\mathbf{r}_d$  nor the direction of  $\mathbf{v}_\times$ . After these adjustments are applied to all members of the merger sample the resulting tracks are over-plotted in the upper frame of Fig. 4. Additionally the edge on sight of all the merging events is presented in the lower panel of this figure. The single tracks in Fig. 3 show the two progenitors approaching each other until they merge together in a jump-like manner. This behaviour is due to the application of the FoF algorithm for the identification of the clusters. The jumps of  $\sim 1 h^{-1} \text{Mpc}$  to the merger point reflect roughly the radii of the progenitor halos. The interesting outcome here is that the separation vector connecting the last distinguishable positions of the progenitors is in both cases (upper and lower panels) strongly aligned with  $\mathbf{r}_d$ . In this representation parallel to the y-axis. This picture can be confirmed by looking at the average plot Fig. 4. The two branches depicting the incoming progenitor halos show enhanced densities slightly left of  $x = 0$ . The connection line between this two areas is parallel to the y-axis. Thus the  $\mathbf{r}_d$  gives a good approximation of the main infall direction. Additionally the tendency of the encounters to be parabolic

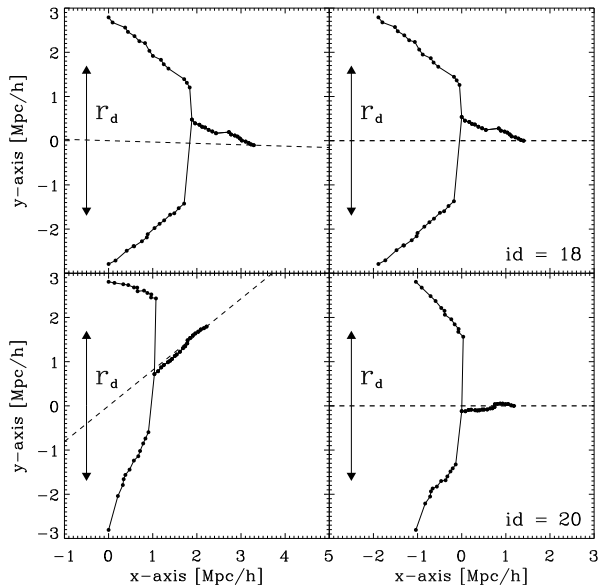


**Figure 3.** Two examples of the adjustment of the merging tracks are shown. The dots indicate the comoving coordinates of the centres of mass found by FoF in a sequence of 33 snapshots between  $z = 0.5$  and  $z = 0$ . The tracks are projected in the plane spanned by the locations of the two most massive progenitors at  $z = 0.5$  ( $\mathbf{r}_1, \mathbf{r}_2$ ) and the position of the cluster at  $z = 0$  ( $\mathbf{r}_0$ ). On the left panels the orbital plane is adjusted in such a way that the x-coordinates of the progenitors at  $z = 0.5$  equal 0 and the y-coordinates show the same distance to the origin. In the panels on the right the fusion point of the two progenitor tracks is shifted towards the origin and a correction for the motion in y-direction is applied. This correction does not affect the orientation of  $\mathbf{r}_d$ , which represents the orientation of connection line between  $\mathbf{r}_1$  and  $\mathbf{r}_2$ .

can be inferred from the average shape of the infall pattern. This behaviour is in agreement with the very detailed investigation by Khochfar & Burkert (2003). The flatness of the distribution of tracks in the edge on representation (lower panel of Fig. 4) indicates that  $\mathbf{v}_\times$  describes the orbital plane in a rather satisfactory manner. These outcomes confirm that despite the apparent simplifications the vectors  $\mathbf{r}_d$  and  $\mathbf{v}_\times$  are capable of determining the direction of infall and the orbital plane, respectively.

### 3.1.1 Impact of infall pattern on clusters' shape

In this paragraph we investigate the correlations between vectors  $\mathbf{r}_d$  and  $\mathbf{v}_\times$  and the shapes of the current clusters. The shape of a cluster is determined by the eigenvectors of the second moment of mass tensor  $\theta$  as given by the following equation.

$$\theta_{ij} = \sum_{k=1,N} m_k(\mathbf{r}_k) r_{ki} r_{kj} \quad (3)$$

Here  $m_k$  specifies the particle masses. The position vector  $\mathbf{r}$  of the  $N$  CDM particles belonging to the halo is given in respect of the centre of mass and the components of the vector belonging to the  $k$ th particle are denoted  $r_{ki}$  for  $i = 1, 3$ . Here we show only the results based on the dark matter component, but the behaviour of the gaseous component is

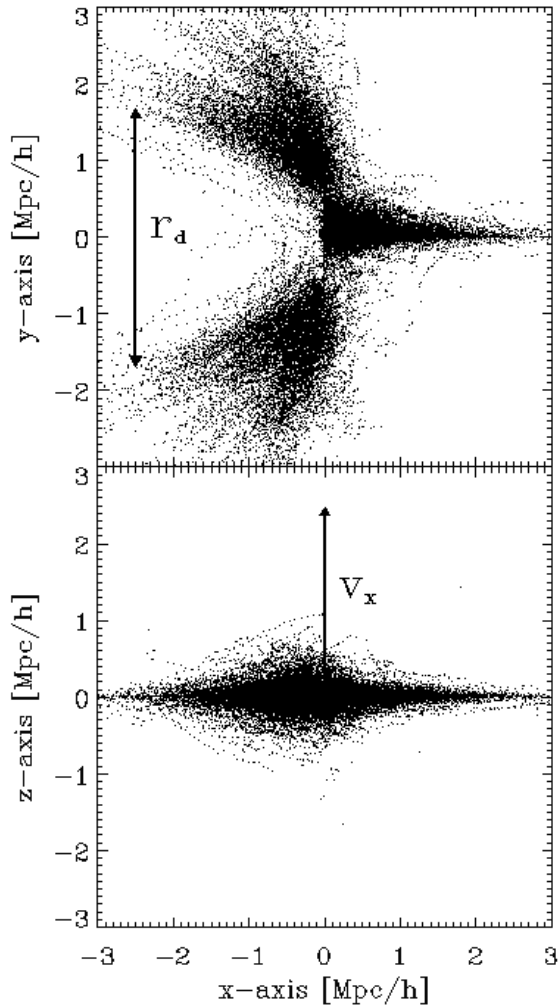


**Figure 4.** The traces of two most massive progenitors ending in the clusters of the merger sample are overlaid after an adjustment procedure like sketched in Fig.(4) has been applied.

very similar. Subsequently the three eigenvectors of  $\theta$  are denoted  $\mathbf{a}$ ,  $\mathbf{b}$  and  $\mathbf{c}$ . The eigenvalues  $a$ ,  $b$  and  $c$  are ordered by magnitude ( $a \geq b \geq c$ ). Hence  $\mathbf{a}$  indicates the major,  $\mathbf{b}$  the intermediate and  $\mathbf{c}$  the minor axis. Clusters show preferentially prolate shape (see e.g. Faltenbacher et al. (2002)) so  $\mathbf{a}$  can be identified with the orientation of the cluster.

First we compute the distributions of the angles between the principal axes and  $\mathbf{r}_d$ . The diagonal in Fig. 5 represents the cumulative distribution of the *cosine* of the angles between two randomly orientated vectors. A curve lying below the diagonal indicates an correlation between vectors, i.e. the vectors have a tendency to be parallel more often than a random sample. A curve lying above the diagonal indicates a anti-correlation between the vectors, i.e. the vectors have a tendency to be more often perpendicular than in a random sample. The thick solid, dashed and dotted lines depict the cumulative distributions of the angles between  $\mathbf{r}_d$  and the principal axes  $\mathbf{a}$ ,  $\mathbf{b}$  and  $\mathbf{c}$  as indicated. The left panel shows the results for the recent major merger sample and the right panel those for the steady accretion mode sample. The dashed lines which represent the angles between the ma-

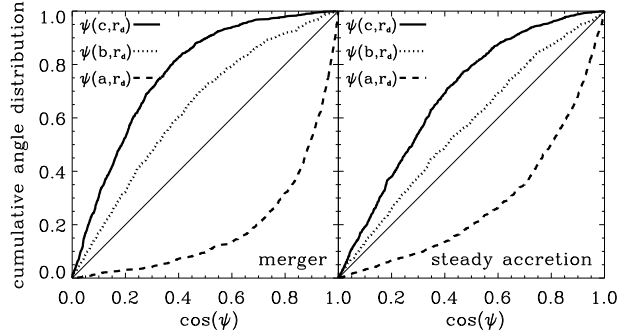


**Figure 5.** The cumulative distribution of the absolute values of the *cosine* between the difference vector  $\mathbf{r}_d$  at  $z = 0.5$  and the the principal axes  $\mathbf{a}$  (dashed),  $\mathbf{b}$  (dotted) and  $\mathbf{c}$  (solid) of the cluster at  $z = 0$  is shown. The diagonal indicates the shape of a random distribution. The left panel gives the result from the merger sample and the right panel shows the outcome for the steady accretion mode sample.

$\psi$	merger	steady
$(\mathbf{c}, \mathbf{r}_d)$	$\lesssim 10^{-45}$	$\lesssim 10^{-45}$
$(\mathbf{b}, \mathbf{r}_d)$	$1.4 \times 10^{-43}$	$1.7 \times 10^{-8}$
$(\mathbf{a}, \mathbf{r}_d)$	$\lesssim 10^{-45}$	$\lesssim 10^{-45}$

**Table 1.** Results of a Kolmogorov-Smirnov test comparing the angle distributions indicated in the first column derived from the recent major merger sample (second column) and the steady accretion mode sample with the random distributions as imaged in Fig. 5.

for principal axis  $\mathbf{a}$  and  $\mathbf{r}_d$  deviate most significantly from a randomly generated distribution (diagonal). These graphs indicate that there is a strong trend for  $\mathbf{a}$  to be orientated parallel to  $\mathbf{r}_d$ . The result of a Kolmogorov-Smirnov (KS) test, comparing these distributions with the random distribution, is given in Tab. 1. The opposite is found for the distributions associated with the two smaller principal axes. They clearly show a trend to be perpendicular to  $\mathbf{r}_d$ . The KS probabilities that the actual distributions are accidental realizations of a random process fall below  $10^{-45}$ . This confirms that the distributions are not due to random processes. The general behaviour is equal for the distributions related to the two different samples (merger/steady). However, the distributions of the merger sample show enhanced deviations from random. The shape of clusters which underwent a major merging event since  $z = 0.5$  is significantly dominated by the pattern of infall, expressed by the vector  $\mathbf{r}_d$ . Since the results of the steady accretion mode sample show qualitatively equal behaviour, we conclude that the orientation of clusters are determined in a more general sense by the mass accretion along the filaments of the cosmic network.

As mentioned above the second vector quantity,  $\mathbf{v}_x$ , is perpendicular to the plane of infall and parallel to the orbital angular momentum of the two progenitors. In Fig. 6 the solid, dotted and dashed lines correspond to the distributions of the angles between  $\mathbf{v}_x$  and the minor, the intermediate and the major axis. Again the deviation from

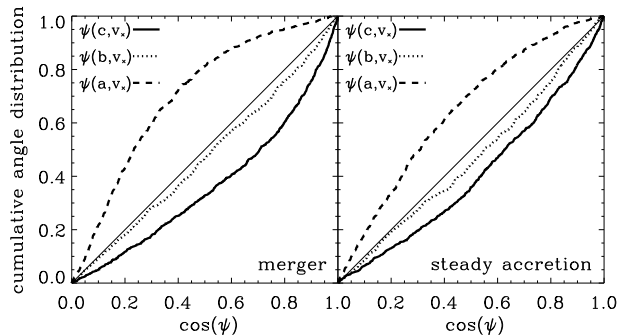


**Figure 6.** The cumulative distribution of the absolute values of the *cosine* between the cross product  $v_{\times}$  of the two infall velocities  $v_1$  and  $v_2$  and the the principal axes **a** (dashed), **b** (dotted) and **c** (solid) of the cluster at  $z = 0$  is imaged. The diagonal indicates the shape of a random distribution. The left panel gives the result from the recent major merger sample and the right panel shows the outcome for the steady accretion mode sample.

$\psi$	merger	steady
$(\mathbf{c}, \mathbf{v}_{\times})$	$3.1 \times 10^{-40}$	$1.3 \times 10^{-18}$
$(\mathbf{b}, \mathbf{v}_{\times})$	$1.4 \times 10^{-3}$	$3.5 \times 10^{-4}$
$(\mathbf{a}, \mathbf{v}_{\times})$	$\lesssim 10^{-45}$	$2.3 \times 10^{-39}$

**Table 2.** Results of a Kolmogorov-Smirnov test comparing the angle distributions indicated in the first column derived from the recent major merger sample (second column) and the steady accretion mode sample with the random distributions as plotted in Fig. 6.

a randomly generated angle distribution (diagonal) is obvious. The most significant deviation from random is seen for  $\psi(\mathbf{a}, \mathbf{v}_{\times})$ , whereas  $\psi(\mathbf{b}, \mathbf{v}_{\times})$  are almost compatible to random orientations. The KS test results are displayed in Tab. 2. The shape of the distributions indicate, that the major axis is perpendicular to  $\mathbf{v}_{\times}$ , whereas the minor axes tend to be in parallel with  $\mathbf{v}_{\times}$ . The distributions associated with the merger events show a more prominent deviation from the random for  $\psi(\mathbf{a}, \mathbf{v}_{\times})$  and  $\psi(\mathbf{c}, \mathbf{v}_{\times})$  and a slightly more random like distribution for  $\psi(\mathbf{b}, \mathbf{v}_{\times})$  compared to the steady accretion mode sample. However (as seen before in the  $\mathbf{r}_d$  distributions) the similarity of the  $\mathbf{v}_{\times}$  distributions indicates that the mass accretion along the filaments is the predominant factor in the determination of the orientation, no matter which accretion mode (merger/steady) is considered.

### 3.1.2 Impact of infall pattern on clusters' angular momentum

Another interesting vector quantity closely related to the dynamics of a halo is the angular momentum. However we want to emphasise at this point that the spin parameter  $\lambda$  of halos is roughly 0.05, which means that the rotational support against gravity is only about 5%. The angular mo-

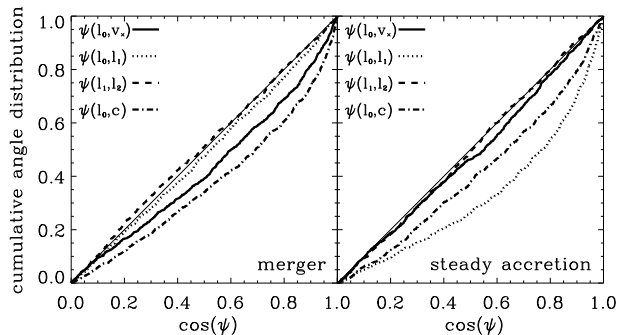


**Figure 7.** The cumulative distribution of the absolute values of the *cosine* between; 1. the angular momentum vector  $\mathbf{l}_0$  at  $z = 0$  and the cross product  $\mathbf{v}_{\times}$  of the two infall velocities  $v_1$  and  $v_2$  at  $z = 0.5$  (solid line), 2.  $\mathbf{l}_0$  and the minor principal axis **c** (dashed-dotted), 3.  $\mathbf{l}_0$  and the angular momentum vector  $\mathbf{l}_1$  of the most massive progenitor at  $z = 0.5$  (dotted line), 4.  $\mathbf{l}_1$  and the the angular momentum vector  $\mathbf{l}_2$  of the second most massive progenitor at  $z = 0.5$  (dashed line). The diagonal indicates the shape of a random distribution. The left panel gives the result from the recent major merger sample and the right panel shows the outcome for the steady accretion mode sample.

mentum for a FoF cluster is computed in the following way.

$$\mathbf{l} = \sum_{i=1, N} m_k \mathbf{r}_i \times \mathbf{v}_i \quad (4)$$

The  $\mathbf{r}$  denotes the particle positions relative to centre of mass,  $m_k$  is the particle mass and  $N$  is the number of particles belonging to the halo. As discussed above the vector  $\mathbf{v}_{\times}$  is perpendicular orientated to the infall plane. If the angular momentum  $\mathbf{l}_0$  of the emerged cluster at  $z = 0$  is dominated by the orbital angular momentum of two most massive progenitors, then a correlation between  $\mathbf{v}_{\times}$  and  $\mathbf{l}_0$  is expected. Therefore we analyse subsequently the distribution of the angles between  $\mathbf{l}_0$  and  $\mathbf{v}_{\times}$ . Additionally we consider the angular momenta of the two progenitor halos  $\mathbf{l}_1$  and  $\mathbf{l}_2$ , where  $\mathbf{l}_1$  corresponds to the angular momentum of the most massive and  $\mathbf{l}_2$  to the second most massive progenitor. In Fig. 7 the various angle distributions connected to the different angular momenta are displayed. Since we have found a strong correlation between  $\mathbf{v}_{\times}$  and **c** (minor axis of the cluster) we also show  $\psi(\mathbf{l}_0, \mathbf{c})$  using dashed-dotted lines. On the left hand side the results for the merger sample are depicted and the outcome for the steady accretion mode sample is displayed on the right panel. The according KS test results comparing these distributions with the random distributions (diagonals in Fig. 7) are presented in Tab. 3. The distributions between the angular momenta of the two progenitors  $\psi(\mathbf{l}_1, \mathbf{l}_2)$  agree with random orientations for both samples.  $\psi(\mathbf{l}_0, \mathbf{c})$  also shows similar behaviour, indicating that  $\mathbf{l}_0$  tends to be parallel to **c**. Here the KS probabilities are enhanced for the merger sample, but the qualitative trend is similar in the steady accretion mode sample. The most obvious differences between the two samples are seen in  $\psi(\mathbf{l}_0, \mathbf{v}_{\times})$  and  $\psi(\mathbf{l}_0, \mathbf{l}_1)$ . These distributions show opposite behaviour for the merger and the steady accretion mode sample. In the merger sample the KS probabilities for  $\psi(\mathbf{l}_0, \mathbf{v}_{\times})$  are very low, indicating that this distribution is obviously incompatible with a random distribution. Instead  $\psi(\mathbf{l}_0, \mathbf{l}_1)$  is almost in agreement with a random distribution.

$\psi$	merger	steady
$(\mathbf{v}_\times, \mathbf{l}_0)$	$2.1 \times 10^{-13}$	$8.1 \times 10^{-3}$
$(\mathbf{l}_0, \mathbf{l}_1)$	$7.4 \times 10^{-2}$	$\lesssim 10^{-45}$
$(\mathbf{l}_1, \mathbf{l}_2)$	$3.4 \times 10^{-1}$	$7.5 \times 10^{-1}$
$(\mathbf{l}_0, \mathbf{c})$	$1.0 \times 10^{-35}$	$2.3 \times 10^{-17}$

**Table 3.** Results of a Kolmogorov-Smirnov test comparing the angle distributions indicated in the first column derived from the recent major merger sample (second column) and the steady accretion mode sample with the random distributions as presented in Fig. 7.

The opposite picture arises in the steady accretion mode sample. Here  $\psi(\mathbf{l}_0, \mathbf{l}_1)$  is clearly not in agreement with a random distribution, whereas  $\psi(\mathbf{l}_0, \mathbf{v}_\times)$  can't be differentiated from random.

We find the effect of steady accretion on the angular momentum is in line with previous work (ie. Vitvitska et al. 2002). If there is no major merger, the angular momentum of the most massive progenitor will be aligned with the angular momentum of the descendant cluster. As seen in Fig. 1, the most massive progenitor in the steady accretion sample is orders of magnitude larger than all other infalling halos. This explains the result for  $\psi(\mathbf{l}_0, \mathbf{l}_1)$ . In the same line of reasoning no strong correlation between angular momentum  $\mathbf{l}_0$  and  $\mathbf{v}_\times$  is expected.

In the merger sample the orbital angular momentum of the two most massive progenitors shows a strong impact on the angular momentum of the descendant. A decided difference between  $\psi(\mathbf{l}_0, \mathbf{v}_\times)$  and a random distribution can be seen. The KS probability of  $2.1 \times 10^{-13}$  strongly discounts any random process as being the origin of this distribution. The tendency for  $\mathbf{l}_0$  and  $\mathbf{v}_\times$  to be parallel confirms the picture that a large fraction of the descendant's angular momentum was gained from the orbital angular momentum of the two most massive progenitors. Whereas the correlation of  $\mathbf{l}_1$  and  $\mathbf{l}_0$  is in agreement with random orientations as can be seen by the rather high value of the KS test.

#### 4 CORRELATIONS IN ORIENTATION AND ANGULAR MOMENTUM

In this section the spatial extent of the correlation in orientation and angular momentum of the  $z = 0$  cluster pairs is evaluated for the whole sample as well as for the two subsamples (merger/steady) separately. To study the alignment effects we use the normalised vector quantities  $\mathbf{v}$  with  $|\mathbf{v}| = 1$ . The distance vector between two clusters is given by  $\mathbf{r}$  with absolute value  $r$ . The normalised distance vector is denoted by  $\hat{\mathbf{r}} = \mathbf{r}/r$ . We investigate the filamentary  $\mathcal{F}_\mathbf{v}(r)$  alignment (see also Faltenbacher et al. 2002) using the following expression.

$$\mathcal{F}_\mathbf{v}(r) = \frac{1}{2} \langle |\mathbf{v}_1 \cdot \hat{\mathbf{r}}| + |\mathbf{v}_2 \cdot \hat{\mathbf{r}}| \rangle_{\mathbf{P}}(r), \quad (5)$$

where  $\langle \rangle_{\mathbf{P}}$  denotes the average over all pairs with separation  $r$ . Due to the spatial symmetry the absolute values of these scalar products are used.  $\mathcal{F}(r)$  quantifies the filamentary

alignment of the vectors  $\mathbf{v}_1$  and  $\mathbf{v}_2$  with the line connecting both clusters.  $\mathcal{F}(r)$  is proportional to the mean value of the cosine of the angles between  $\mathbf{v}_1$  and the vector  $\hat{\mathbf{r}}$  connecting the pairs. Random orientations imply  $\mathcal{F}(r) = 0.5$ . Since the distribution of angles is not of Gaussian shape around a given mean value, it would be wrong to apply Gaussian statistics to estimate the errors. Thus, to investigate the  $1\sigma$  confidence intervals we perform a non-parametric Monte Carlo test (Besag & Diggle 1977; Gottlöber et al. 2002; Kerscher et al. 2001; Kerscher 1998). Here the null hypothesis is “no deviation from random angles”. We simulate this null hypotheses by keeping the positions of the halos fixed and randomly re-assigning the orientations to the halos. This procedure is repeated 99 times. The rms-deviation for these realisations gives a measure for the  $1\sigma$  confidence interval for the given data set. These intervals are indicated by the shaded areas around the expected values for random distributions in Figs. 8, 9 and 10. Thus, if  $\mathcal{F}(r)$  lies outside of this intrinsic scatter region around 0.5 the deviation from random orientations is confirmed at a  $1\sigma$  confidence level. In addition to the alignment of the CDM component we present the alignment signals for the gaseous halos. Recently Kazantzidis et al. (2004) have shown, that the elongation of halos is reduced by dissipative processes like radiative cooling of the gas at the cluster centre. Since we use adiabatic simulations this effect is not represented. However according to Eq. 3 the second moment of mass tensor  $\theta$  and thus the orientations of the principal axes are dominated by the mass distribution on the outskirts of the clusters. Moreover, we are mainly concerned with the orientation of the halo, not the actual axial ratios, and the orientation is not affected by dissipative effects.

#### 4.1 Correlation of clusters' orientations

In this section the filamentary correlation of the orientation of cluster pairs is investigated. Therefore we replace  $\mathbf{v}$  in Eq. 5 with the major (and subsequently the minor principal) axes.

$$\mathcal{F}_\mathbf{p}(r) = \frac{1}{2} \langle |\mathbf{p}_1 \cdot \hat{\mathbf{r}}| + |\mathbf{p}_2 \cdot \hat{\mathbf{r}}| \rangle_{\mathbf{P}}(r) \quad (6)$$

Here  $\mathbf{p}_1$  and  $\mathbf{p}_2$  denote the principal axes (major or minor) of a cluster pair at  $z = 0$  and the associated separation vector  $\mathbf{r}$ . The analysis is done for the whole cluster sample and for the two sub-samples (merger/steady) separately. The results for the alignment of the major and the minor axes are shown in Fig. 8 and Fig. 9, respectively.

A  $\mathcal{F}(r) > 0.5$  indicates that the axes tend to be aligned with the connecting line of the clusters. For the basic cluster sample, comprising the 3000 most massive clusters in the simulation volume, this signal for the major axes extends up to  $100 h^{-1} \text{Mpc}$  (left panel of Fig. 8). The behaviour of the CDM and the gaseous component show very similar behaviour. For the merger and the steady accretion mode samples the signal extends up to  $80 h^{-1} \text{Mpc}$ . Again there is no distinctive difference between the CDM and the gaseous component. The somewhat shorter range appears to be a result of the lower statistics (only 1000 members per sub-sample) rather than caused by the different accretion modes.

A  $\mathcal{F}(r) < 0.5$  indicates that the axes tend to be perpendicular orientated to the connecting line of the cluster

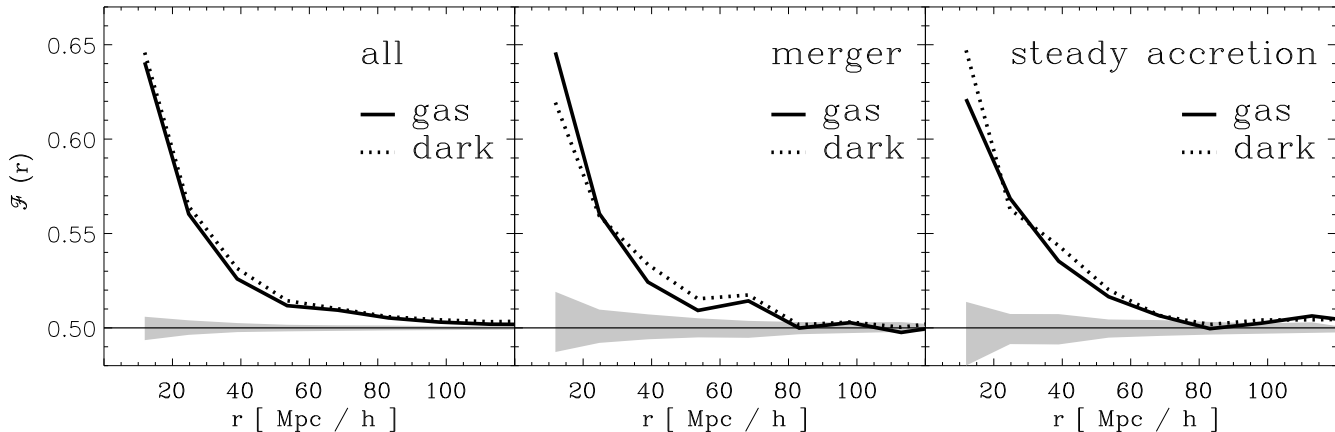


**Figure 8.** This figure shows the mean values of the *cosine* between the clusters’ major axis and the connecting line pointing to another cluster in reference to the distance (length of the connecting line) of the cluster pair. The solid lines indicate the signal achieved for the gaseous component and the dotted lines describes the behaviour of the CDM component. The horizontal solid line gives the expected values for a random distribution of the orientations. The shaded area is a measure of the intrinsic scatter of the signal it is obtained by repeatedly randomising the orientations among the clusters. The three panels from right to left image the results for the whole, the merger and the steady accretion sample, respectively.

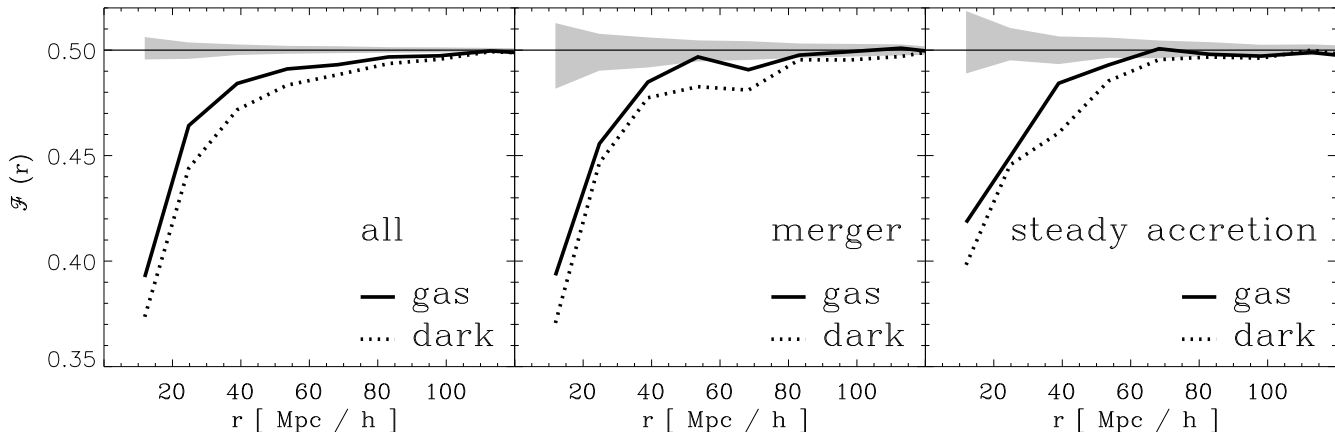


**Figure 9.** Here the mean values of the *cosine* between the clusters’ minor axis and the connecting line pointing to another cluster in reference to the distance (length of the connecting line) of the cluster pair are plotted. The solid lines indicate the signal achieved for the gaseous component and the dotted lines describes the behaviour of the CDM component. The horizontal solid line gives the expected values for a random distribution of the orientations. The shaded area is a measure of the intrinsic scatter of the signal it is obtained by repeatedly randomising the orientations among the clusters. The three panels from right to left image the results for the whole, the merger and the steady accretion sample, respectively.

pairs. For the basic cluster sample, the signal for the minor axis extends up to  $80 h^{-1} \text{Mpc}$  (left panel of Fig. 9). This result is in good agreement with Bailin & Steinmetz (2004), where a strong tendency for the minor axes of halos to lie perpendicular to the large scale filaments is found. The signal of the CDM component is slightly enhanced compared to the gaseous component. The CDM component of the recent major merger sample (middle panel of Fig. 9) shows a similar range whereas the gaseous component is comparable to random orientations at separations of  $\sim 60 h^{-1} \text{Mpc}$ . The alignment signal for both components of the steady accretion mode sample extends up to  $\sim 60 h^{-1} \text{Mpc}$ . Again the shorter correlation ranges for the sub-samples might be caused by

the smaller size of the sub-samples. However the enhanced signal for the CDM component in all three samples might originate in the different physical properties of the CDM and the gaseous components.

In the previous section we show that the infall of halos is correlated with the orientation of the cluster and is independent of accretion mode. In this section we also show that the orientations of clusters are correlated and independent of accretion mode. Since the steady accretion mode sample shows just as much correlation as the merger mode sample all progenitors must be falling in along the same relative direction. From this, we conclude that the alignment is strongly supported by infall along filamentary structure. The correlation

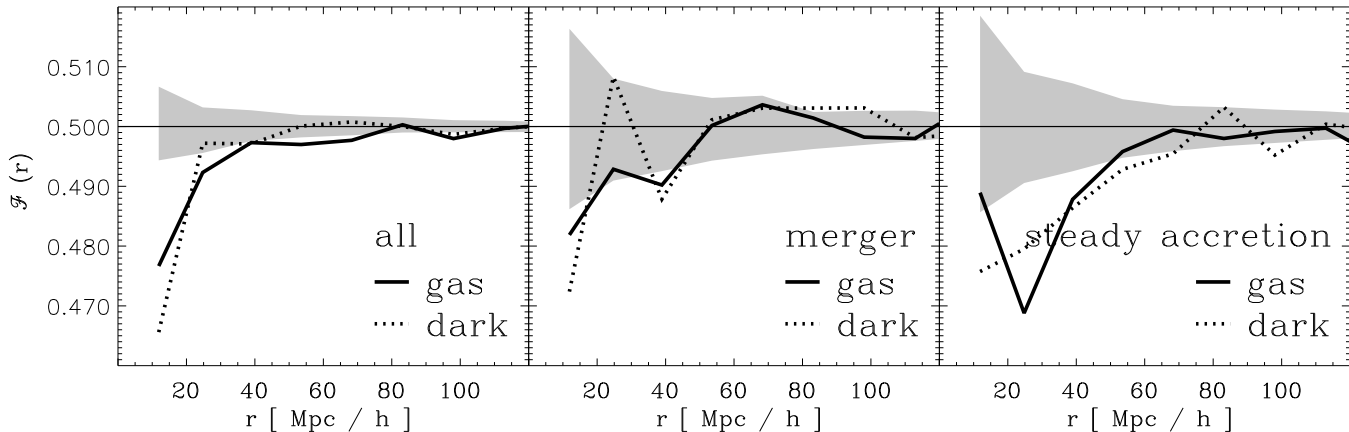


**Figure 10.** The solid lines indicate the signal for the gaseous component and the dotted lines describes the behaviour of the CDM component.

length ( $\lesssim 100 h^{-1}\text{Mpc}$ ) for cluster alignment that we find in our simulation is in agreement with the findings of Hopkins et al. (2005).

#### 4.2 Alignment of clusters' angular momenta

In §3.1.2 we analyse the effects of different accretion modes on the angular momentum of current clusters. We find a different behaviour in the merger and the steady accretion mode samples. Therefore we now investigate the correlation of the intrinsic angular momenta of cluster pairs in the whole sample, as well as in the two sub-samples. The angular momenta are inserted into equation (5).

$$\mathcal{F}_1(r) = \frac{1}{2} \langle |\mathbf{l}_a \cdot \hat{\mathbf{r}}| + |\mathbf{l}_b \cdot \hat{\mathbf{r}}| \rangle_P(r) \quad (7)$$

Here  $\mathbf{l}_a$  and  $\mathbf{l}_b$  denote the normalised angular momenta of a cluster pair separated by the spatial vector  $\mathbf{r}$ . The result of this study is displayed in Fig. 10. Similar to the result for the correlation of the minor axes (see Fig. 9) the angular momenta show the trend to be perpendicular orientated to the connecting lines. Thus they tend to be perpendicular to the filaments as well. However the signal reaches only out to separations of  $\sim 20 h^{-1}\text{Mpc}$  for the complete sample. The signal in the recent major merger sample is hardly distinguishable from random fluctuations. Apart from the innermost data point for the gaseous component the signal in the steady accretion mode shows the largest extension  $\lesssim 60 h^{-1}\text{Mpc}$ . However the deviation from random is far smaller than seen in the correlations of the principal axes. As mentioned in the beginning of §3.1.2, ordered rotation supports the halo against gravitational collapse only at a 5% level, thus a low deviation from random is expected. The interesting point here is the rather long range for the steady accretion mode sample compared to the almost disappearing signal for the merger sample. It is assumed that all halos go through a merger phase (rapid mass growth) prior to a steady accretion phase (see eg. Wechsler et al. 2002). Therefore, on average the merger sample is younger than the steady accretion sample. The natural conclusion from the above observations combined with those of the previous

section is that infall along the filaments tends to torque the halo's angular momentum into a perpendicular orientation with respect to those filaments. This is supported by the fact that the merger sample is still in a phase of rapid accretion, major mergers impart large amounts of angular momentum, and the mergers will happen preferentially along the filament. It is expected that the merger sample will settle down in time and reflect the same sort of correlations as the current steady accretion sample. We plan on addressing this issue in a soon to be forthcoming paper Allgood et al. (2005).

## 5 SUMMARY

We use large scale N-body simulations, including gas dynamics (GADGET) within the standard  $\Lambda\text{CDM}$  model ( $\Omega_m = 0.3$ ,  $\Omega_\Lambda = 0.7$ ,  $h = 0.7$ ) to investigate the mass accretion statistics and the correlation of orientation and angular momentum of galaxy clusters. The basic cluster sample comprises the 3000 most massive FoF clusters found in the CDM distribution at  $z = 0$ . These objects span a mass range between  $1.1 \times 10^{14} h^{-1}M_\odot$  and  $2.3 \times 10^{15} h^{-1}M_\odot$  (plus  $\approx 15\%$  gas). For all of the clusters in the sample we have located the two most massive progenitors at  $z = 0.5$ . Based on the mass fractions of these two progenitors  $m_2/m_1$  ( $m_1 \geq m_2$ ) two cluster subsamples were constructed, a merger sample containing the 1000 clusters with highest  $m_2/m_1$  values and a steady accretion mode sample with the 1000 lowest  $m_2/m_1$  values. For the recent major merger sample a average fraction  $(m_1 + m_2)/m_0$ , where  $m_0$  denotes the  $z = 0$  mass of the cluster, of 0.57 is found, whereas for the steady accretion mode sample a value of 0.75 is obtained. The clusters which have two nearly equal mass progenitors at  $z = 0.5$  tend to accrete more matter in addition to  $m_1 + m_2$  than the clusters in the steady accretion mode. Hence major mergers happen predominantly in regions of averagely enhanced mass accretion.

To gain insight into the infall pattern of merging events we followed the 2000 progenitors related to the merger sample using 33 snapshots between  $z = 0.5$  and  $z = 0$ . On aver-

age the infall patterns are not complex. The merging takes place parallel to the connecting vector  $\mathbf{r}_d$  of the progenitor halos at  $z = 0.5$ . Despite the relatively high additional mass accretion the tracks of the two progenitors and the descendant are reasonably well confined within the plane defined by  $\mathbf{v}_\times$ . Thus the tracks do not twine each other, instead the two most massive progenitors approach each other in a fairly straight manner, until the outskirts overlap and the FoF algorithm is not able to discriminate between them. We find that the orientation and the angular momentum of the clusters at  $z = 0$  are tightly correlated with the vectors  $\mathbf{r}_d$  and  $\mathbf{v}_\times$ . Namely  $\mathbf{r}_d$  tends to be parallel to the major axis and perpendicular to the minor axis of the emerged cluster and the opposite behaviour is found for  $\mathbf{v}_\times$ . Comparing these results to the steady accretion mode clusters, we find similar but slightly less significant correlations. This behaviour indicates that the current orientation is a result of mass flows along the filaments onto the cluster, independent of whether this happens in a steady accretion or a merger mode. However the effects on the angular momentum are different in the two sub-samples. The angular momenta  $\mathbf{l}_0$  of the clusters in the merger sample show the tendency to be parallel to  $\mathbf{v}_\times$ , whereas the orientation of the intrinsic angular momenta of the most massive progenitors  $\mathbf{l}_1$  at  $z = 0.5$  has a minor influence on the angular momentum at  $z = 0$ . The opposite picture arises in the steady accretion mode sample. Here  $\mathbf{l}_0$  and  $\mathbf{l}_1$  are correlated, whereas the angle distribution between  $\mathbf{l}_0$  and  $\mathbf{v}_\times$  is in agreement with random orientations.

The correlations found in the orientations between cluster pairs confirm the previous results. The major axes of cluster pairs tend to be parallel to their connecting line for distances up to  $80 h^{-1}\text{Mpc}$  no matter whether the steady accretion or the merger sample is under consideration. Furthermore the minor axes of cluster pairs tend to be oriented perpendicular to the connecting line for cluster separations of the same extend. A signal up to  $100 h^{-1}\text{Mpc}$  is found, when the whole sample of 3000 clusters is considered. The mass accretion along the filaments appears to be responsible for the signal, no matter which accretion mode is under consideration. Slight correlations for angular momentum are seen only in the complete and the steady accretion mode sample. The angular momenta tend to be orthogonal to the connecting lines of cluster pairs up to  $20 h^{-1}\text{Mpc}$  for the complete and up to  $60 h^{-1}\text{Mpc}$  for the steady accretion mode sample. We conclude that merging along filamentary structures is responsible for the tendency of the angular momentum to be perpendicular to the filaments. This effect is stronger in the steady accretion sample because the halos in this sample have already gained all of their angular momentum from infall along the filaments. The merger sample is still in a phase of accretion and additional infall along the filaments will bring the merger sample into agreement with the current steady accretion sample. The correlations in the orientations and the angular momenta for the gas and the dark matter components show very similar behaviour, supporting the search for alignment effects in large X-ray samples of clusters of galaxies. Since adiabatic gas dynamics are employed here, this outcome may change slightly with the application of a more accurate treatment of gas dynamics. However additional dissipative gas physics will mainly affect the shape of the halos but not erase the orientation completely.

## ACKNOWLEDGEMENTS

The authors would like to thank William G. Mathews and Joel Primack for insightful comments. BA is supported by a NASA grant (NAG5-12326) and a NSF grant (AST-0205944). GY thanks M.E.C (Spain) for financial support under projects AYA-2003-07468 and BFM2003-01266. GY and SG thanks the Acciones Integradas Hispano-Alemanas for support. YH has been supported by the Israel Science Foundation grant 143/02. The simulations were performed at the John von Neumann Institute for Computing Jülich.

## APPENDIX A: COMMENTS ON HALO TRACING SCHEME

Tracing halos through a number of simulation outputs is a subtle task. Most merger tracing algorithms use particle association in order to construct potential progenitor and descendant relationships. This is not enough to determine the exact relationship. Often there are more than one potential progenitors or descendants to choose from and further criteria must be met in order to identify the true relationship. Most approaches use some a priori fixed thresholds (like: *the mass of the progenitor must lie above a certain percentage of the current mass*) which lead to reasonable results but may break down if none of the potential candidates meets the criteria. Here we present a complementary approach, which avoids problems which come about by using rigid limits. It is a maximisation process where the best candidate is the halo which leads to the highest value returned from A1. Therefore this procedure does not run the risk of breaking down due to hard limits.

$$\alpha = \left[ 1 - \frac{|m_a - m_b|}{m_a + m_b} \right] \times \frac{m_o}{m_a} \quad (\text{A1})$$

$m_a$  and  $m_b$  are the masses of the progenitor halo and descendant candidates respectively.  $m_o$  denotes the mass of particles which are found in both of the halos.

The above expression can be split up into two parts. The first part evaluates whether progenitor and descendant have similar masses, the second part expresses the overlap of particles in both the progenitor and descendant halos. The **first** part framed by the square brackets, results in values close to 1 if the mass of the progenitor  $m_a$  and mass of the descendant candidate  $m_b$  are similar. This behaviour is expected if the time-steps between the simulation outputs are reasonably short and there is no ongoing major merging event. The **second** part of Eq. A1 ( $m_o/m_a$ ) gives the ratio between the mass of overlap particles and the mass of the progenitor halo. If there has been no major merging event, this fraction should be close to 1 if the right descendant candidate is under consideration. Thus both parts of equation result in values close to 1 if the right descendant is found and therefore  $\alpha$  is close to 1. Whereas wrong candidates tend to result in small values of  $\alpha$  since the overlap might be small and/or the masses of progenitor and (assumed) descendant might differ strongly.

During major merging events the situation is more complicated, but the maximisation procedure still ensures that the most probable descendant is chosen. Lastly it should be emphasised, that this method has the ability to trace halos in both directions, both backwards and forwards in time.

**REFERENCES**

- Allgood B., Flores F., Primack J. R., A. F., R. W., 2005  
Bailin J., Steinmetz M., 2004  
Besag J., Diggle P. J., 1977, *Appl. Statist.*, 26, 327  
Binggeli B., 1982, *A&A*, 107, 338  
Binney J., Silk J., 1979, *MNRAS*, 188, 273  
Chambers S. W., Melott A. L., Miller C. J., 2002, *ApJ*, 565, 849  
Colberg J. M., White S. D. M., Yoshida N., MacFarland T. J., Jenkins A., Frenk C. S., Pearce F. R., Evrard A. E., Couchman H. M. P., Efstathiou G., Peacock J. A., Thomas P. A., The Virgo Consortium 2000, *MNRAS*, 319, 209  
Doroshkevich A. G., 1973, *ApL*, 14, 11  
Faltenbacher A., Gottlöber S., Kerscher M., Müller V., 2002, *A&A*, 395, 1  
Gottlöber S., Kerscher M., Kravtsov A. V., Faltenbacher A., Klypin A., Müller V., 2002, *A&A*, 387, 778  
Hopkins P. F., Bahcall N. A., Bode P., 2005, *ApJ*, 618, 1  
Jenkins A., Frenk C. S., White S. D. M., Colberg J. M., Cole S., Evrard A. E., Couchman H. M. P., Yoshida N., 2001, *MNRAS*, 321, 372  
Kazantzidis S., Kravtsov A. V., Zentner A. R., Allgood B., Nagai D., Moore B., 2004, *ApJ*, 611, L73  
Kerscher M., 1998, *A&A*, 336, 29  
Kerscher M., Mecke K., Schuecker P., Böhringer H., Guzzo L., Collins C. A., Schindler S., De Grandi S., Cruddace R., 2001, *A&A*, 377, 1  
Khochfar S., Burkert A., 2003, submitted to *MNRAS*; astro-ph/0309611  
Onuora L. I., Thomas P. A., 2000, *MNRAS*, 319, 614  
Peebles P. J. E., 1980, *The Large Scale Structure of the Universe*. Princeton: Princeton University Press  
Plionis M., 1994, *ApJS*, 95, 401  
Plionis M., Benoist C., Maurogordato S., Ferrari C., Basilakos S., 2003, *ApJ*, 594, 144  
Porciani C., Dekel A., Hoffman Y., 2002a, *MNRAS*, 332, 325  
Porciani C., Dekel A., Hoffman Y., 2002b, *MNRAS*, 332, 339  
Rhee G. F. R. N., Latour H. J., 1991, *A&A*, 243, 38  
Richstone D., Loeb A., Turner E. L., 1992, *ApJ*, 393, 477  
Springel V., Yoshida N., White S. D. M., 2001, *New Astronomy*, 6, 79  
Suwa T., Habe A., Yoshikawa K., Okamoto T., 2003, *ApJ*, 588, 7  
Ulmer M. P., McMillan S. L. W., Kowalski M. P., 1989, *ApJ*, 338, 711  
van Haarlem M. P., Frenk C. S., White S. D. M., 1997, *MNRAS*, 287, 817  
Vitvitska M., Klypin A. A., Kravtsov A. V., Wechsler R. H., Primack J. R., Bullock J. S., 2002, *ApJ*, 581, 799  
Wechsler R. H., Bullock J. S., Primack J. R., Kravtsov A. V., Dekel A., 2002, *ApJ*, 568, 52  
West M. J., 1994, *MNRAS*, 268, 79  
West M. J., Blakeslee J. P., 2000, *ApJ*, 543, L27  
White S. D. M., 1984, *ApJ*, 286, 38